The acute nociceptive signals induced by bradykinin in rat sensory neurons are mediated by inhibition of M-type K$^+$ channels and activation of Ca^{2+}-activated Cl$^−$ channels

Boyi Liu, … , Hailin Zhang, Nikita Gamper

Research Article

Bradykinin (BK) is an inflammatory mediator and one of the most potent endogenous pain-inducing substances. When released at sites of tissue damage or inflammation, or applied exogenously, BK produces acute spontaneous pain and causes hyperalgesia (increased sensitivity to potentially painful stimuli). The mechanisms underlying spontaneous pain induced by BK are poorly understood. Here we report that in small nociceptive neurons from rat dorsal root ganglia, BK, acting through its B$_2$ receptors, PLC, and release of calcium from intracellular stores, robustly inhibits M-type K$^+$ channels and opens Ca^{2+}-activated Cl$^−$ channels (CaCCs) encoded by *Tmem16a* (also known as *Ano1*). Summation of these two effects accounted for the depolarization and increase in AP firing induced by BK in DRG neurons. Local injection of inhibitors of CaCC and specific M-channel openers both strongly attenuated the nociceptive effect of local injections of BK in rats. These results provide a framework for understanding spontaneous inflammatory pain and may suggest new drug targets for treatment of such pain.

Find the latest version:

The acute nociceptive signals induced by bradykinin in rat sensory neurons are mediated by inhibition of M-type K⁺ channels and activation of Ca²⁺-activated Cl⁻ channels

Boyi Liu,[1,2] John E. Linley,[2] Xiaona Du,[1] Xuan Zhang,[1]
Lezanne Ooi,[2] Hailin Zhang,[1] and Nikita Gamper[2]

[1]Department of Pharmacology, Hebei Medical University, Shijiazhuang, China. [2]Institute of Membrane and Systems Biology,
Faculty of Biological Science, University of Leeds, United Kingdom.

Bradykinin (BK) is an inflammatory mediator and one of the most potent endogenous pain-inducing substances. When released at sites of tissue damage or inflammation, or applied exogenously, BK produces acute spontaneous pain and causes hyperalgesia (increased sensitivity to potentially painful stimuli). The mechanisms underlying spontaneous pain induced by BK are poorly understood. Here we report that in small nociceptive neurons from rat dorsal root ganglia, BK, acting through its B₂ receptors, PLC, and release of calcium from intracellular stores, robustly inhibits M-type K⁺ channels and opens Ca²⁺-activated Cl⁻ channels (CaCCs) encoded by *Tmem16a* (also known as *Ano1*). Summation of these two effects accounted for the depolarization and increase in AP firing induced by BK in DRG neurons. Local injection of inhibitors of CaCC and specific M-channel openers both strongly attenuated the nociceptive effect of local injections of BK in rats. These results provide a framework for understanding spontaneous inflammatory pain and may suggest new drug targets for treatment of such pain.

Introduction

Bradykinin (BK) has long been known as one of the most potent endogenous pain-inducing (algogenic) substances (1, 2), and it is a major inflammatory mediator (3). BK and related short peptides (kinins) are produced de novo at sites of injury or inflammation from their precursors, kininogens, by serine proteases such as tissue kallikrein or by proteases released from mast cells and basophils (4). Cellular effects of BK are mediated by specific receptors, B₁ and B₂. B₁ receptors are usually absent from noninflamed tissues and have a low affinity for BK; thus, it is believed that the majority of the acute effects of BK are mediated by B₂ receptors (B₂Rs), which are G protein–coupled receptors acting via G_{q/11} signaling cascades (5).

When applied exogenously to a human skin blister or injected into arteries supplying viscera in laboratory animals (1), BK induces two major effects: (a) severe spontaneous pain and (b) increased sensitivity to painful (hyperalgesia) and nonpainful (allodynia) thermal and mechanical stimuli (2, 5). The latter effect has attracted considerable attention and is now relatively well understood. It is believed that B₂R activation induces sensitization of sensory ion channels, including TRPV1 (6) and TRPA1 (7). Additional mechanisms for BK-induced hyperalgesia are mediated by PKCε (8), which in turn also causes TRPV1 sensitization (9). Unfortunately, the understanding of the molecular events underlying acute pain directly induced by BK is not that advanced and is mostly based on the electrophysiological observations of BK-induced depolarization (10, 11), increased action potential (AP) firing (12), and inward current induction (10, 12). BK has

been referred to as "the most potent endogenous algogenic substance known" (2); thus, the elucidation of its modes and mechanisms of action should improve our ability to understand and treat spontaneous inflammatory pain.

The aim of this study was to investigate the mechanisms of acute nociceptive signaling induced by BK. We characterized the major membrane currents directly affected by BK in nociceptive sensory neurons of dorsal root ganglia (DRG), investigated their molecular identities, the signaling cascades that regulate them, and their contribution to neuronal excitability and to BK-induced nocifensive behavior in rats. Our findings indicate that the major effects of BK on the excitability of nociceptors are mediated by PLC- and Ca²⁺-dependent inhibition of M-type K⁺ channels and by simultaneous opening of Ca²⁺-activated Cl⁻ channels (CaCCs) encoded by transmembrane protein 16A (*Tmem16a*). Both these effects contribute to membrane depolarization in primary sensory afferents, resulting in the generation of ascending nociceptive signals. Thus, this study presents a step-by-step reconstitution of the molecular events of the acute nociceptive signal induced in the peripheral sensory system by BK. Our findings also put forward new candidate drug targets for the treatment of inflammatory pain.

Results

Signaling pathways triggered in DRG neurons by BK. It is well established that the most abundant BK receptors, B₂, couple to G_{q/11} and activate PLC (5). PLC hydrolyzes the plasma membrane phospholipid phosphatidylinositol 4,5-bisphosphate (PIP₂) and releases inositol 1,4,5-trisphosphate (IP₃) into the cytosol; the latter can then trigger exit of Ca²⁺ from IP₃-sensitive intracellular stores. Both PIP₂ depletion and Ca²⁺ release are powerful signaling events capable of regulating neuronal ion channels. However, Ca²⁺
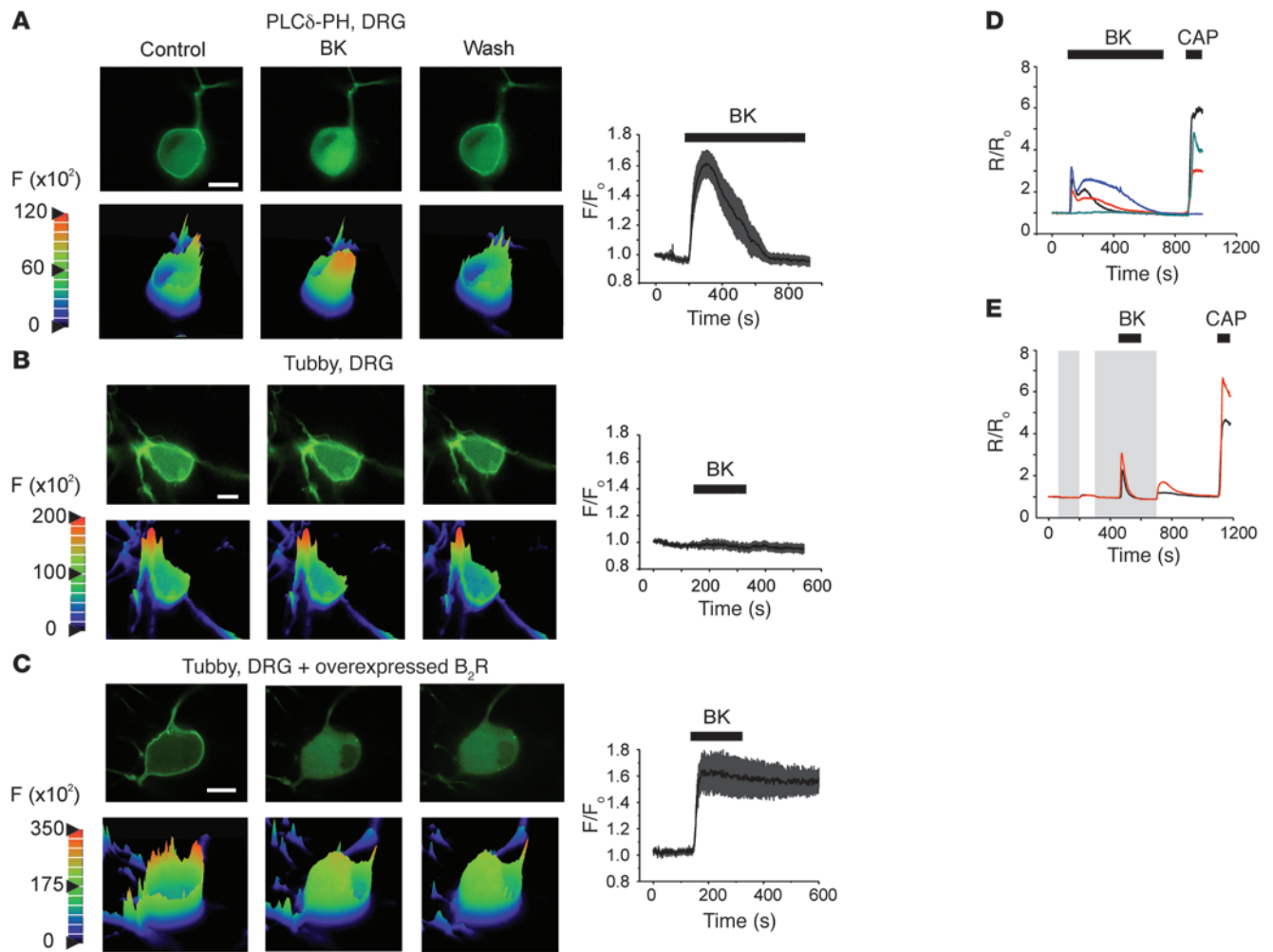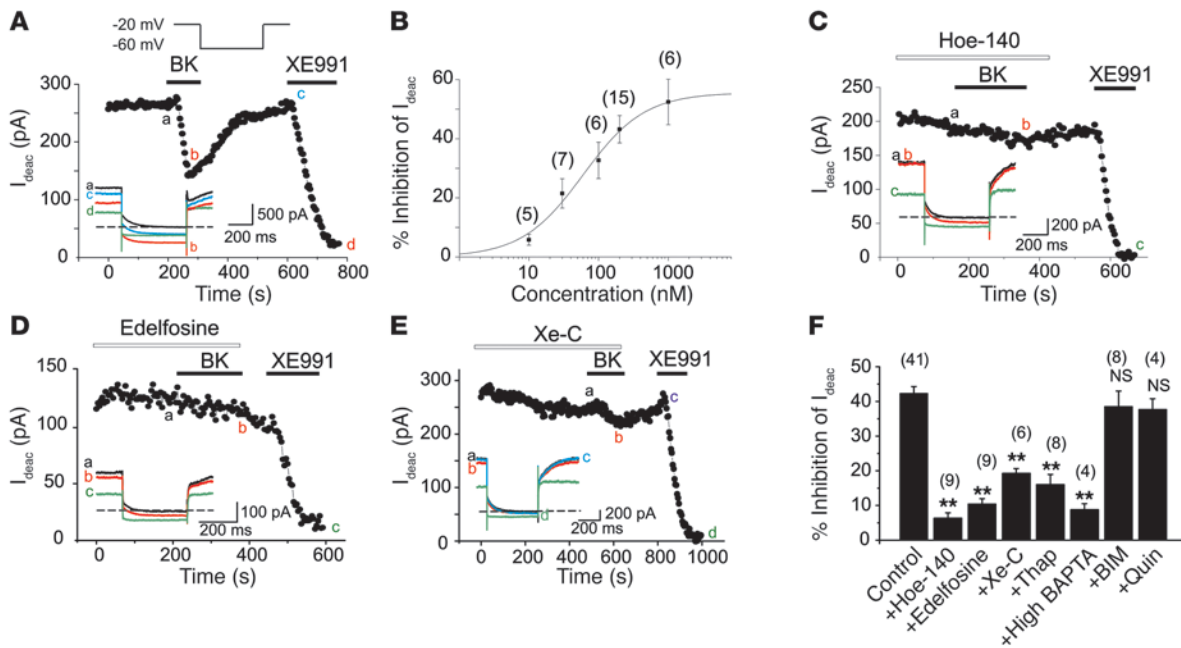
Figure 1
Characterization of BK-induced signaling in DRG neurons. (**A**) BK-induced translocation of the IP$_3$/PIP$_2$ probe PLCδ-PH-GFP, overexpressed in DRG neurons. Top panels show confocal micrographs of the transfected neuron before (Control), during (BK), and after (Wash) the application of 200 nM BK. Lower panels show the corresponding surface intensity plots. Color scale is absolute pixel intensity (×10^2). The plot on the right shows mean (±SEM) relative increase in cytosolic fluorescence in 8 DRG neurons during BK application (indicated by the bar). (**B**) As in **A**, but using YFP-tubby probe; n = 11. (**C**) As in **B**, but neurons were cotransfected with B$_2$R cDNA (F/F$_0$). Scale bars in **A**–**C**: 10 μm. (**D** and **E**) BK-induced Ca^{2+} signals in DRG neurons. (**D**) [Ca^{2+}]$_i$ was measured in small DRG neurons loaded with fura-2AM as normalized ratio (R/R_0) of fluorescence at 340 and 380 nm. BK (200 nM) and CAP (1 μM) were applied during periods indicated by the bars. (**E**) Experiment similar to that shown in **D**, but Ca^{2+}-free extracellular solution was applied (as indicated by the shaded areas) before and during the BK application.

release after PLC activation does not always occur; likewise, localized hydrolysis of PIP$_2$ does not always lead to a global drop in the membrane PIP$_2$ level (13, 14). Our initial approach was therefore to examine these first steps of the BK signaling cascade in DRG.

In the first series of experiments, we transfected DRG neurons with PLCδ-PH-GFP, a fluorescent probe containing the PIP$_2$-binding domain from PLCδ fused to GFP. This probe binds to PIP$_2$ (15) and IP$_3$ (for which the probe has higher affinity; refs. 16, 17). As shown in the confocal images in Figure 1A, under basal conditions, the PLCδ-PH-GFP probe localized predominantly to the plasma membrane. Application of 200 nM BK produced a strong, reversible translocation of the probe to the cytosol (manifested by a 1.6 ± 0.08–fold rise in cytosolic fluorescence, n = 8; Figure 1A) in 8 of 14 small neurons (soma diameter, 20–30 μm; typical neurons selected for confocal and electrophysiological experiments are

shown in Supplemental Figure 1A; supplemental material available online with this article; doi:10.1172/JCI41084DS1). This result suggests that PLC is activated and PIP$_2$ is hydrolyzed upon BK stimulation in DRG neurons. However, since PLCδ-PH-GFP has a higher affinity for IP$_3$ than for PIP$_2$, translocation of the probe does not necessarily indicate a significant drop in membrane PIP$_2$ levels, as even small amounts of hydrolyzed PIP$_2$ may produce enough IP$_3$ to cause the probe to translocate (13, 18). Thus, we used a new PIP$_2$ probe (YFP-tubby, R332H mutated), which does not bind IP$_3$ (19), to probe whether there was a significant depletion of the membrane PIP$_2$ pool. Like PLCδ-PH-GFP, the YFP-tubby also localized predominantly to the plasma membrane (Figure 1B); however, unlike PLCδ-PH-GFP, YFP-tubby failed to translocate to the cytosol after BK application in 11 of 12 neurons tested (see also Supplemental Figure 2). BK, however, induced a robust translocation of the YFP-
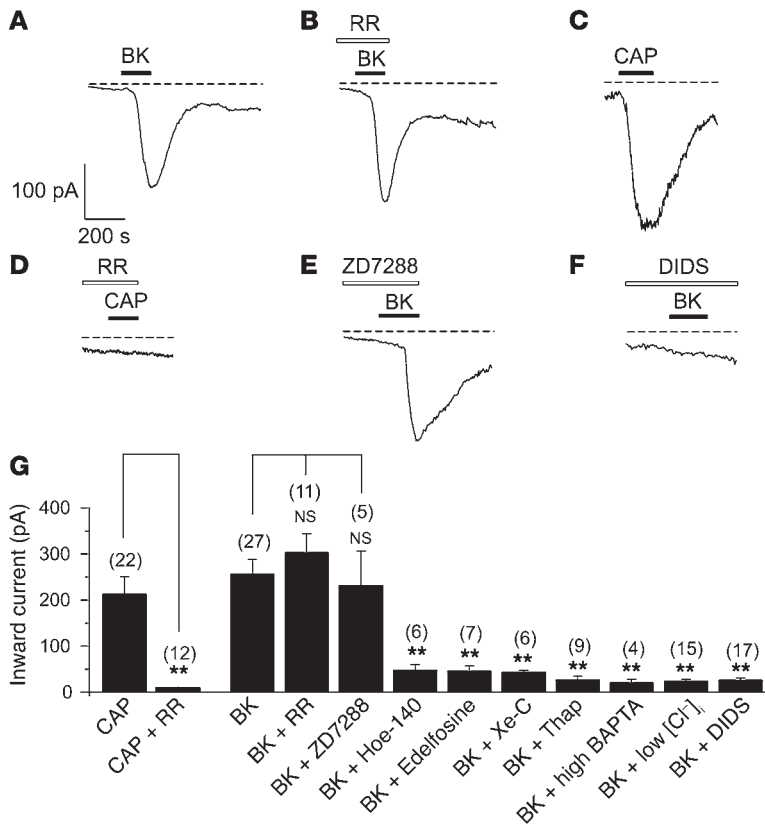
Figure 2

BK inhibits M current in DRG neurons. (**A**) Time course for the effect of 200 nM BK on M current amplitude (I_{deac}, the amplitude of the deactivating tail current at –60 mV; see Methods). A specific M channel blocker, XE991 (3 μM), was applied at the end of the recording. Drugs were applied during the periods indicated by the bars. The lower inset shows the current traces recorded at the times indicated by the letters; the dotted line indicates a zero current level. The voltage protocol is depicted in the inset above. (**B**) Concentration dependency of the inhibitory effect of BK on M current. The curve represents the fit of data to a logistic equation (see Methods). The *n* number for each data point is given in parentheses. (**C–E**) As in **A**, but neurons were pretreated with (**C**) the specific B$_2$R antagonist Hoe-140 (100 nM), (**D**) PLC inhibitor edelfosine (10 μM), or (**E**) IP$_3$ receptor blocker xestospongin C (Xe-C, 1 μM). (**F**) Summary of the pharmacology of BK-induced M current inhibition. Bars show percentage M current inhibition by 200 nM BK (Control); BK + 100 nM Hoe-140; BK + 10 μM edelfosine; BK + 1 μM Xe-C; BK + 2 μM thapsigargin (Thap); BK + high BAPTA pipette solution; BK + 100 nM bisindolylmaleimide (BIM); and BK + 10 μM quinacrine (Quin). The number of experiments is given above each bar; **$P \leq 0.01$.

tubby in DRG neurons cotransfected with the probe and exogenous B$_2$R (Figure 1C), suggesting that this probe is capable of reporting BK-induced PIP$_2$ depletion when it is strong enough. These results suggest that although BK clearly causes PIP$_2$ hydrolysis and IP$_3$ generation in DRG neurons (Figure 1A), membrane PIP$_2$ levels do not drop to a significant enough degree to induce translocation of the YFP-tubby probe, possibly because endogenous PIP$_2$ levels are high and/or well buffered in DRG neurons.

We then performed Ca^{2+} imaging experiments to test whether BK application produces Ca^{2+} signals in DRG neurons. In fura-2AM–loaded neurons (preidentified by their response to bath application of 30 mM KCl), 200 nM BK induced prominent Ca^{2+} signals in 155 of 252 neurons tested (Figure 1D). These signals were usually biphasic, with a sharp transient rise followed by a slower and smaller secondary elevation (Figure 1D). Removal of extracellular Ca^{2+} abolished the secondary responses but not the initial transient one (Figure 1E), suggesting that the first, transient phase of the signal was predominantly due to Ca^{2+} release from intracellular stores, while the second, slower phase was due to Ca^{2+} influx pathways (see below). In all Ca^{2+} imaging experiments, we applied the TRPV1 agonist capsaicin (CAP, 1 μM) at the end to identify TRPV1-positive nociceptors; 174 of 252 neurons were CAP positive; 107 of 155 BK-responsive neurons were CAP positive.

BK inhibits M current in small DRG neurons. Previous studies revealed that (a) BK induces membrane depolarization in cultured small DRG neurons (10–12); and (b) these neurons express several M-type K$^+$ channel subunits (Kv7.2, Kv7.3, and Kv7.5; ref. 20), whose inhibition induces depolarization and increases AP firing (21, 22). Since M channels can be inhibited via PLC pathways (reviewed in ref. 23), we investigated whether BK affects M current in cultured nociceptive DRG neurons. We identified nociceptors by size and morphology (Supplemental Figure 1A) and by their sensitivity to 1 μM CAP. M currents were recorded by amphotericin B–perforated patch-clamp using a voltage protocol depicted in Figure 2A (inset) and measured as the deactivation tail current amplitude when the membrane voltage was stepped from –20 to –60 mV. Bath application of BK (10 nM–1 μM) caused a concentration-dependent inhibition of M current (Figure 2B) in the majority of the tested neurons, with an EC$_{50}$ of 60.0 ± 16.3 nM. The mean inhibition of M current by 200 nM BK amounted to 43.2% ± 4.6% (*n* = 15) and could be partially reversed upon washout (Figure 2A). We used a specific M channel blocker, XE991 (3 μM), to verify the identity of the deactivation current (Figure 2A and thereafter); XE991 abolished the deactivation tail currents by 96.5% ± 2.1% (*n* = 56). In a representative population of 47 small neurons recorded under the same conditions, 28 of 47 were CAP positive, 44 of 47 were BK positive, and 26 of 28 CAP-positive neurons were BK positive. The larger proportion of BK-positive cells seen in the patch-clamp versus Ca^{2+} imaging experiments is likely due to the different selection procedure: small "peanut-shaped" neurons (Supplemental Figure 1A) were selected for patch clamp, while imaging was carried out with total neurons in the optical field.
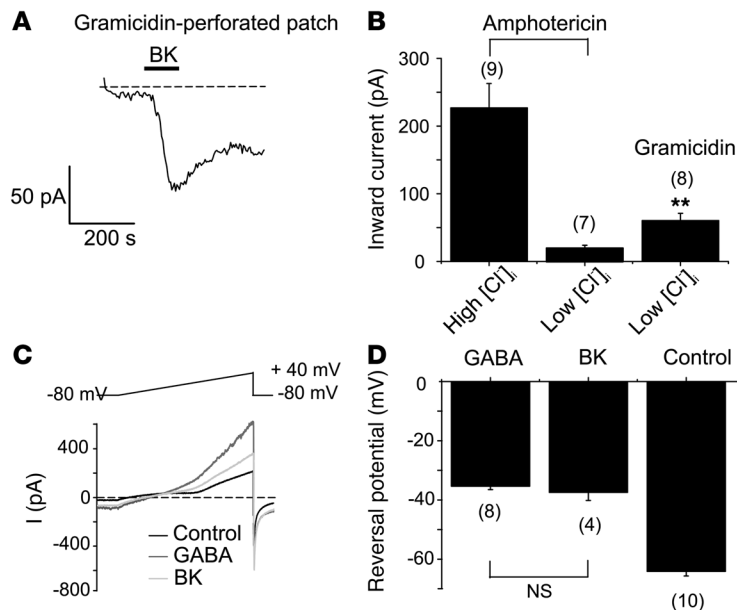
Figure 3
BK induces Ca^{2+} activated CaCC in DRG neurons. (**A**–**F**) Representative current traces showing inward currents induced by BK (200 nM) and CAP (1 µM). Traces were obtained by continuous recording at a holding potential of −60 mV. Dotted lines indicate zero current level. Timing of the BK and CAP application is indicated by black bars; white bars indicate pretreatment with 10 µM Ca^{2+} channel blocker RR (**B** and **D**), 10 µM HCN blocker ZD7288 (**E**), and 100 µM Cl^- channel blocker DIDS (**F**). (**G**) Summary for the pharmacology of the BK-induced inward current in DRG. Bars show the peak inward current amplitude induced by the following substances: 1 µM CAP; CAP + 10 µM RR; 200 nM BK; BK + 10 µM RR; BK + 10 µM ZD7288; BK + 100 nM Hoe-140; BK + 10 µM edelfosine; BK + 1 µM Xe-C; BK + 2 µM thapsigargin; BK + high BAPTA pipette solution; BK + low $[Cl^-]_i$ pipette solution; BK + 100 µM DIDS. The number of experiments is given above each bar in parentheses; **$P \le 0.01$.

It has been reported that some BK effects in DRG cultures can be mediated by non-neuronal satellite cells (24); thus, we tested whether the action of BK on M current would also require non-neuronal cells. We prepared purified DRG cultures (Supplemental Figure 3 and Supplemental Methods) and recorded from neurons that were not in physical contact with any surrounding cells (Supplemental Figure 3B). 200 nM BK still induced inhibition of M current by 46.0%±3.0% (n = 8; versus inhibition under normal culture, 45.1%±4.5%, n = 14; P > 0.05; Supplemental Figure 3A). Thus, the action of BK on M current was due to a primary effect on DRG neurons.

Next we tested the significance of the main steps in the B_2R signaling pathway for the BK-induced M current inhibition in DRG nociceptors. Pretreatment of neurons with the B_2R antagonist Hoe-140 (100 nM) and the PLC inhibitor edelfosine (10 µM) abolished M current inhibition (6.3% ± 1.6% and 10.4% ± 1.6% inhibition of M current, n = 9; Figure 2, C, D, and F). BK-induced M current inhibition was also reduced by disruption of intracellular Ca^{2+} signaling: xestospongin C (Xe-C, a membrane-permeable IP_3 receptor antagonist), thapsigargin (a sarco-/endoplasmic reticulum Ca^{2+}-ATPase inhibitor), and chelation of intracellular Ca^{2+} with the high-affinity Ca^{2+} buffer BAPTA (20 mM; 12-minute dialysis in "fast" whole-cell mode) significantly ($P \le 0.01$) reduced M current inhibition (Figure 2, E and F). The PLA_2 inhibitor quinacrine (10 µM) and the PKC inhibitor bisindolylmaleimide (100 nM) were without effect (Figure 2F). In all, the above results suggest that BK-induced M current inhibition depends on the PLC- and IP_3-mediated intracellular Ca^{2+} rises.

BK activates TMEM16A-dependent Cl^- channels. In all our patch-clamp experiments, BK-induced inhibition of M current was always accompanied by the simultaneous activation of an inward

current at −60 mV (e.g., Figure 2A, inset). The kinetics of development of inward current very closely followed that of inhibition and recovery of M current (Supplemental Figure 4); the times for activation and decay of the inward current were 93 ± 4 seconds and 275 ± 16 seconds (n = 24), respectively, and the times for maximal inhibition and recovery of the M current were 95 ± 6 seconds and 272 ± 18 seconds (n = 24), respectively (Supplemental Figure 4). However, inhibition of M current and activation of an inward current were indeed distinct phenomena, as robust inward currents were still seen when BK was applied in the presence of XE991 (Supplemental Figure 5A). We reasoned that this significant inward current is likely to have a depolarizing effect on the membrane potential of neurons and thus may contribute to the excitatory effect of BK. In order to identify this current, we first tested TRP channel involvement, since the sensitizing effect of BK on different sensory neuron–specific TRP channels (e.g., TRPV1, ref. 6; and TRPA1, ref. 7) is well documented. In small DRG neurons voltage-clamped at −60 mV, 200 nM BK evoked inward currents with an average amplitude of −231.1 ± 27.9 pA (Figure 3, A and G, n = 27); 1 µM CAP also induced inward currents of comparable amplitude (−212.7 ± 37.7 pA, n = 22; Figure 3, C and G). The effect of CAP was totally abolished by the broad-spectrum Ca^{2+} channel blocker ruthenium red (RR), as the CAP-evoked current in the presence of 10 µM RR amounted to only −14.2 ± 1.5 pA (n = 12, P ≤ 0.01 compared with CAP alone). In a separate imaging experiment, 10 µM RR also completely abolished Ca^{2+} transients induced by the TRPA1 agonist mustard oil (100 µM, Supplemental Figure 6). In contrast, RR had no effect on the BK-induced inward current (−302.8 ± 41.1 pA in the presence of RR, n = 11; Figure 3, B, D, and G). Thus, we concluded that the BK-evoked inward cur-

Figure 4
Characterization of BK-induced inward currents using gramicidin-perforated patch. (**A**) Representative current trace showing BK-induced (200 nM) inward current in gramicidin-perforated patch using low [Cl$^-$]$_i$ pipette solution. (**B**) Summary statistics for the BK-induced inward currents recorded with amphotericin B (high [Cl$^-$]$_i$ and low [Cl$^-$]$_i$ pipette solutions) and gramicidin (low [Cl$^-$]$_i$ pipette solution). **$P \leq 0.01$ compared with low [Cl$^-$]$_i$ amphotericin B. (**C**) Representative current traces induced in small DRG neuron by the voltage ramp from −80 mV to +40 mV (depicted above the traces) applied on the peak of BK- (200 nM) or GABA-induced (200 μM) currents. (**D**) Mean reversal potentials for BK- and GABA-induced currents recorded as in **C**. The number of experiments is given below each bar.

rent was not conducted by RR-sensitive TRP channels. The inward current was also not affected by the hyperpolarization-activated cyclic nucleotide–gated cation channel (HCN) blocker ZD7288 (10 μM; −231.2 ± 74.9 pA, n = 5; Figure 3, E and G). However, lowering intracellular Cl$^-$ ([Cl$^-$]$_i$) by using a K acetate–based pipette solution (see Methods) almost completely abolished BK-induced inward current (−25.4 ± 4.0 pA, n = 15, P ≤ 0.01 compared with control). The broad-spectrum chloride channel blocker 4,4′-diisothiocyanatostilbene-2, 2′-disulphonic acid (DIDS, 100 μM) also abolished BK-induced inward current (−26.0 ± 4.9 pA, n = 17, P ≤ 0.01 compared with control; Figure 3, F and G). Other Cl$^-$ channel blockers, niflumic acid (NFA, 100 μM; Supplemental Figure 5B) and 5-nitro-2-(3-phenylpropylamino)benzoic acid (NPPB, 100 μM; data not shown), also effectively blocked BK-induced inward currents. The above results suggest that the inward current evoked by BK was almost exclusively due to chloride channel opening.

CaCCs have been reported in DRG neurons (25–27); therefore, we tested whether the BK-induced inward current in DRG neurons was mediated by the same B$_2$R/PLC/Ca^{2+} pathways as the M current inhibition. The B$_2$R antagonist Hoe-140 and PLC blocker edelfosine both prevented the inward current responses (−47.9 ± 11.7 pA, n = 6 and −45.7 ± 11.4 pA, n = 7; both P ≤ 0.01 compared with control; Figure 3G). The BK-induced inward current was also significantly attenuated by treatment with either Xe-C (−57.5 ± 4.4 pA, n = 6, P ≤ 0.01 compared with control; Figure 3G), thapsigargin (−26.2 ± 8.1 pA, n = 9, P ≤ 0.01 compared with control; Figure 3G) or 20 mM BAPTA in fast whole-cell mode (−19.8 ± 7.5 pA, n = 4, P ≤ 0.01 compared with control; Figure 3G), further suggesting that this inward current is conducted by CaCCs activated via the PLC/IP$_3$/Ca^{2+} pathway.

In the experiments described above, we varied [Cl$^-$]$_i$ in neurons using perforated patch recording with the Cl$^-$-permeable pore-forming agent amphotericin B. In order to evaluate the endogenous electrochemical driving force for Cl$^-$, we used gramicidin in the patch pipette, which forms Cl$^-$-impermeable pores (28). First we confirmed that in gramicidin-perforated patch BK still induces inward currents at −60 mV (−65.3 ± 11.1 pA,

n = 8; Figure 4, A and B); the BK-induced inward current recorded in gramicidin-perforated patch in combination with "low [Cl$^-$]$_i$" pipette solution was smaller compared with that recorded with amphotericin B with "high [Cl$^-$]$_i$" pipette solution (Figure 4B) but still substantial. Accordingly, the low [Cl$^-$]$_i$ pipette solution abolished BK-induced inward current when recordings were made with amphotericin B but not with gramicidin (Figure 4B). These data suggest that [Cl$^-$]$_i$ in DRG neurons is high enough to maintain a driving force for inward current at −60 mV. To determine the endogenous reversal potential for Cl$^-$ currents in small DRG neurons, we studied GABA-induced currents in gramicidin-perforated patch. In these experiments, NaCl in the extracellular solution and KCl in the pipette solution were substituted with equimolar tetraethylammonium chloride (TEA-Cl) and CsCl, respectively. In accordance with previously published data (29), 200 μM GABA induced Cl$^-$ currents that reversed at −37.4 ± 2.7 mV; importantly, BK-induced currents reversed at the same potentials (−34.2 ± 4.3 mV; Figure 4, C and D), further supporting our assumption that BK-induced inward currents in small DRG neurons are in fact Cl$^-$ currents.

The gene encoding an essential CaCC subunit (*Tmem16a*) has recently been identified (30–32). Thus, we used siRNA against *Tmem16a* to test whether it is a molecular correlate of the BK-induced Cl$^-$ current in small DRG neurons. Transfection (using a Nucleofector device, Amaxa) of siRNA significantly reduced levels of *Tmem16a* mRNA (Figure 5F; Supplemental Figure 7, C and D) and protein (Figure 5G and Supplemental Figure 7, A and B), as compared with the levels in acutely dissociated cells and cultures from P7 and adult rats and also as compared with the cultures transfected with the scrambled oligo control. A TMEM16A antibody stained neurons coexpressing TRPV1 and the M channel subunit Kv7.2 but not satellite glial cells (Supplemental Figure 1B and Supplemental Figure 7A). In cells transfected with *Tmem16a* siRNA, TMEM16A but not TRPV1 immunoreactivity was reduced (Supplemental Figure 7A). *Tmem16a* siRNA did not affect expression of *Tmem16b*, which was also expressed in DRG but at a much lower level than *Tmem16a* (Supplemental Figure 7, C and D).
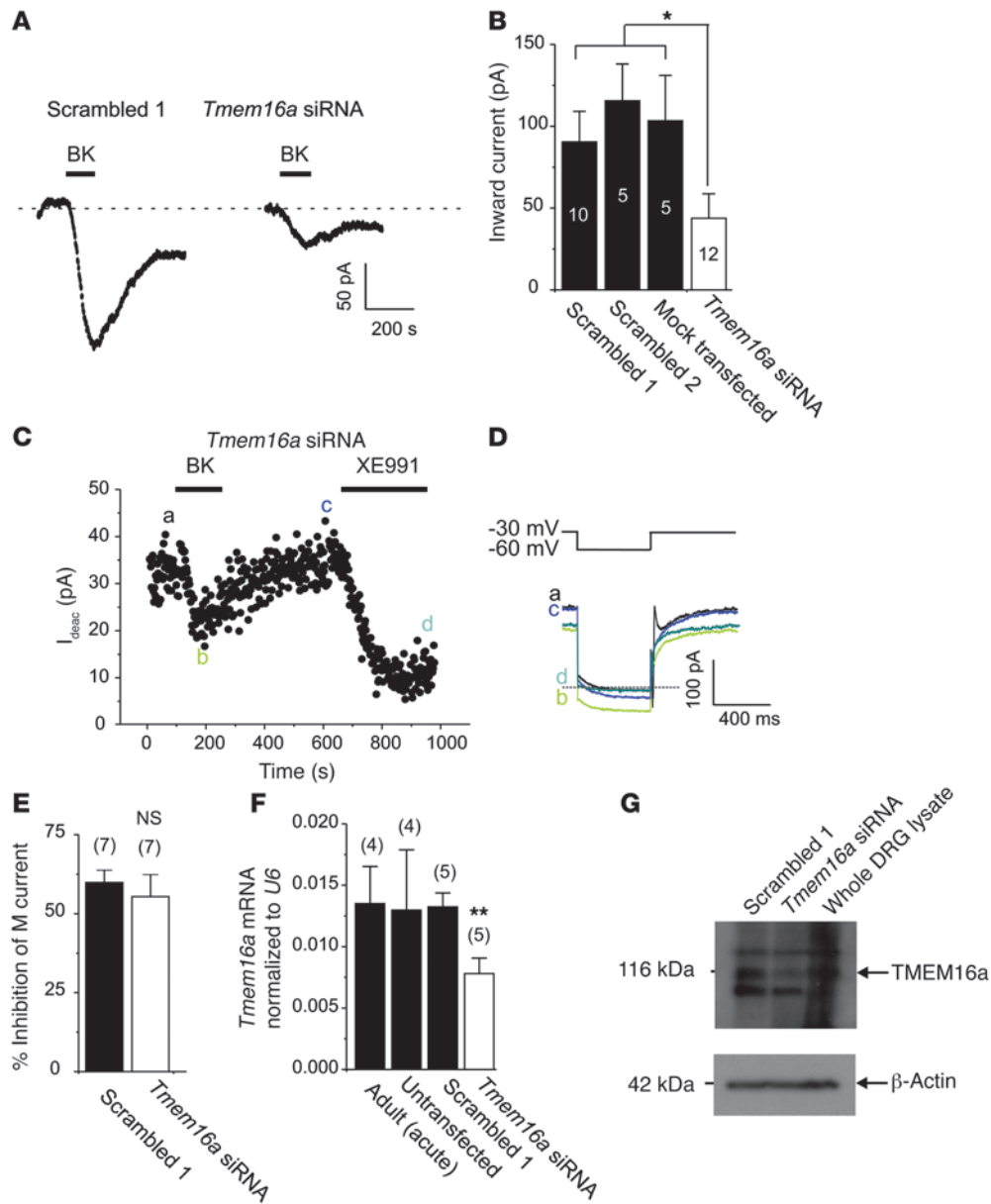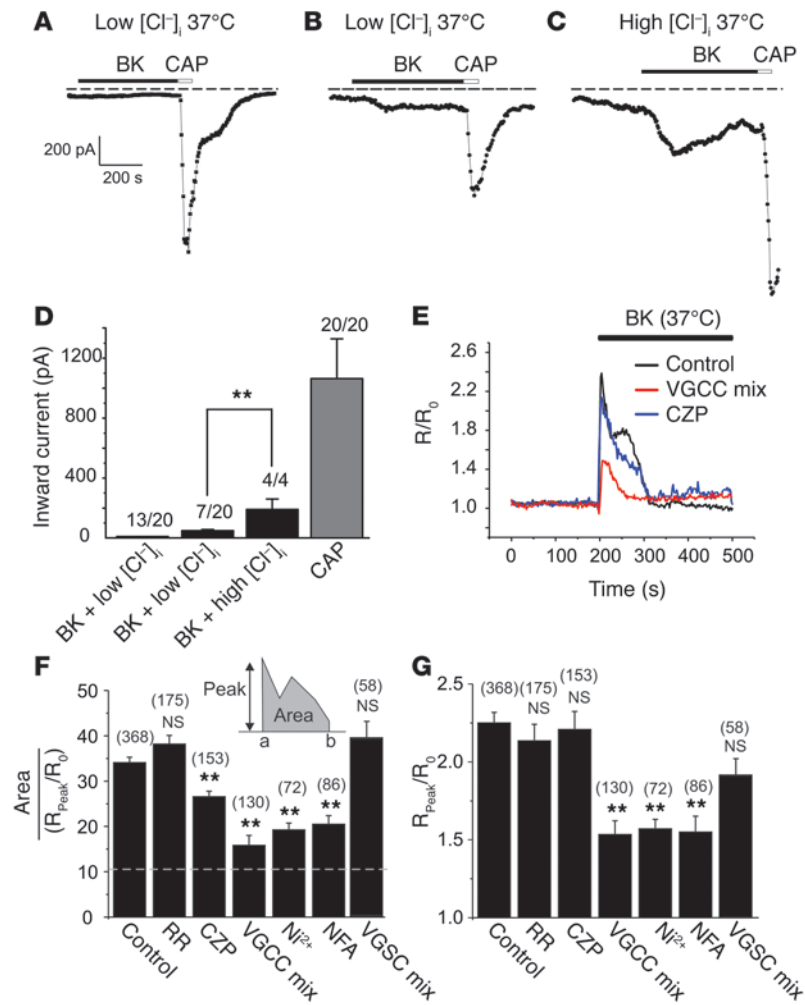
Figure 5
CaCC current in DRG neurons depends on expression of TMEM16A. (**A**) Current at –60 mV induced by BK (200 nM) in small DRG neurons is attenuated by *Tmem16a* siRNA (right trace) but not by the scrambled siRNA control (left trace). (**B**) Mean peak inward current amplitudes for experiments as in **A**, for cells transfected with 2 different scrambled oligos (scrambled 1 and 2), mock-transfected cells, and cells transfected with *Tmem16a* siRNA. *$P \leq 0.05$; numbers of experiments are shown in the bars. (**C**–**E**) *Tmem16a* siRNA does not affect BK-induced inhibition of M current. Application of 200 nM BK to the neuron transfected with *Tmem16a* siRNA induced robust inhibition of M current, which was recorded by the voltage pulse from –30 mV to –60 mV (inset above the current traces in **D**). (**E**) Mean M current inhibition by BK in neurons transfected with scrambled oligos or *Tmem16a* siRNA. (**F**) *Tmem16a* mRNA levels (normalized to the housekeeping gene *U6*) in DRG cultures transfected with scrambled oligo (scrambled 1) or *Tmem16a* siRNA, as well as in untransfected culture and acutely dissociated DRG prep from an adult (8 weeks) rat; **$P \leq 0.01$. (**G**) Western blot showing decrease in TMEM16A protein abundance (band at 116 kDa) in whole cell lysates of DRG cells transfected with *Tmem16a* siRNA (as compared with the scrambled oligo control 1) and whole protein lysate from acutely extracted DRG (no cell culture) of P7 rat; loading control was β-actin.

In small DRG neurons transfected with 2 different scrambled oligos, BK induced a robust inward current with a mean amplitude of -90.5 ± 18.6 pA (scrambled 1, $n = 10$; Figure 6, A and B) and of -115.6 ± 22.5 pA (scrambled 2, $n = 5$; Figure 6B); the amplitude of the BK-induced inward current in mock-transfected neurons (cells were electroporated but without any RNA) was -103.4 ± 27.6 pA ($n = 5$;

Figure 5B). In contrast, neurons transfected with *Tmem16a* siRNA responded to BK with much smaller currents (-43.8 ± 15.0 pA, or 48% of the value for the scrambled 1 oligo control, $n = 12$, $P < 0.05$; Figure 5, A and B). The inward current amplitudes in all variants of transfected controls were smaller than that recorded in nontransfected cells (Figure 3), suggesting some nonspecific

Figure 6
Characterization of BK-induced inward currents and Ca²⁺ transients at 37°C. (**A–C**) Representative current traces showing inward currents at 37°C induced by 200 nM BK and 1 μM CAP. (**A**) In 13 of 20 CAP-positive neurons, BK did not induce inward current during recording with low [Cl⁻]ᵢ pipette solution. (**B**) In 7 of 20 neurons, BK induced small inward currents (low [Cl⁻]ᵢ pipette solution). (**C**) In 4 of 4 CAP-positive neurons, BK induced large inward currents during recording with high [Cl⁻]ᵢ solution. (**D**) Summary for experiments in **A–C**. (**E**) Exemplary Ca²⁺ imaging experiments (similar to that in Figure 1, D and E) at 37°C. BK (1 μM) was applied either alone (Control) or after 5 minutes preincubation with (and in the presence of) 10 μM capsazepine (CZP) or a VGCC-blocking cocktail (1 μM ω-conotoxin GVIA, 100 nM agatoxin TK, 1 μM nifedipine, 50 μM NNC 55-0396). (**F**) Pharmacological characterization of the second-phase Ca²⁺ rises induced by BK. The y axis is the relative area/peak parameter and is a measure of the second-phase Ca²⁺ rise (see Methods and explanation in Results). Bars represent mean area/peak parameter for Ca²⁺ transients induced by BK only (Control) or by BK in the presence of 10 μM RR, 10 μM CZP, VGCC-blocking cocktail, 1 mM NiCl₂ (Ni²⁺), 100 μM NFA or VGSC blockers (1 μM TTX and 100 nM A-803467). (**G**) Bars represent mean normalized peak of ratiometric BK-induced Ca²⁺ signal (R/R_0); all labeling as in **F**. Only CAP- and BK-positive neurons were included in **E** and **F**. The number of cells is given in parentheses. **$P \leq 0.01$.

effects of electroporation; nevertheless, the effect of the siRNA was specific. Furthermore, in neurons with *Tmem16a* knockdown, BK still induced robust inhibition of M current (Figure 5, C–E).

Our data strongly suggest that the BK-induced inward current in small DRG neurons is CaCC; however, BK was also shown to sensitize several sensory TRP channels such as TRPV1 (6) and TRPA1 (7) that, when open, conduct inward cationic currents at negative voltages. Particularly, sensitization of TRPV1 by BK results in a leftward shift of the temperature response curve such that the threshold for channel activation shifts closer toward body temperature (33). We thus performed further patch-clamp and imaging experiments to test the involvement of TRP channels in the acute effects of BK on DRG nociceptors at 37°C. In the majority (13 of 20) of small CAP-positive neurons, BK-induced inward currents were not seen when recorded in amphotericin B–perforated patch mode in combination with low [Cl⁻]ᵢ pipette solution (Figure 6, A and D). In only 7 of 20 CAP-positive neurons, BK induced small non-Cl⁻ inward currents of –48.9 ± 7.5 pA (Figure 6, B and D); these currents were much smaller than those recorded with high [Cl⁻]ᵢ pipette solution (–190.2 ± 69.9 pA, 4 of 4 neurons; Figure 6, C and D). We also tested the effect of BK on DRG neurons overexpressing exogenous B₂Rs. Even with B₂R overexpression, application of BK induced only very small inward currents of –11.24 ± 2.23 pA (n = 8; recordings were made with low [Cl⁻]ᵢ pipette solution in the pres-

ence of 3 μM XE991 at room temperature). As a control for these sets of experiments, we tested whether we could detect BK-induced sensitization of TRPV1 to CAP, and indeed we found that when 2 successive applications of 50 nM CAP were separated by 5 minutes of treatment with 200 nM BK, in 6 of 9 CAP-positive neurons, the second CAP application produced 1.7 ± 0.2–fold larger current than the first CAP application (data not shown). Together, these findings suggest that coupling of endogenous B₂R to sensory TRP channels in small DRG neurons is such that it provides for sensitization but less so for activation of these channels.

We also performed detailed characterization of the BK-induced Ca²⁺ rises at 37°C in imaging experiments (Figure 6, E–G). In order to quantify the contribution of a second-phase response to the total BK-induced Ca²⁺ signal, we calculated the total area under the curve of the ratiometric Ca²⁺ signal and divided it by the peak amplitude of Ca²⁺ signal (see Figure 6F, inset, and Methods); the larger the contribution of the second-phase Ca²⁺ rise to the total Ca²⁺ signal, the higher the value of this area/peak parameter. The dotted line in Figure 6F indicates the predicted value for the area/peak parameter for a single Gaussian peak of amplitude (R/R_0 = 2.25) and time to peak (15 seconds), characteristic of the mean (n = 34) BK-induced Ca²⁺ transient in small CAP-positive DRG neurons (i.e., the value for the mean BK-induced Ca²⁺ peak with no second phase).
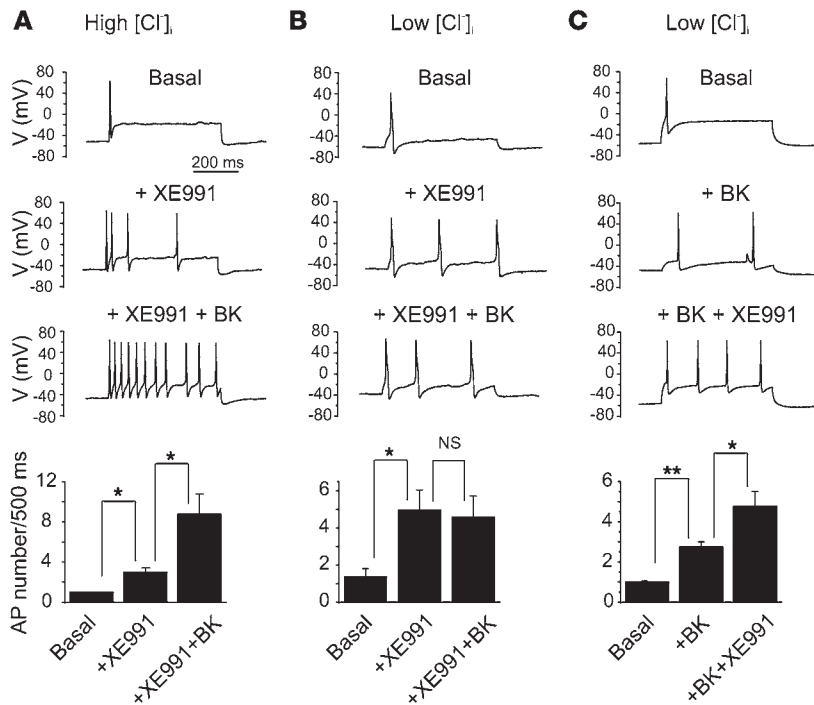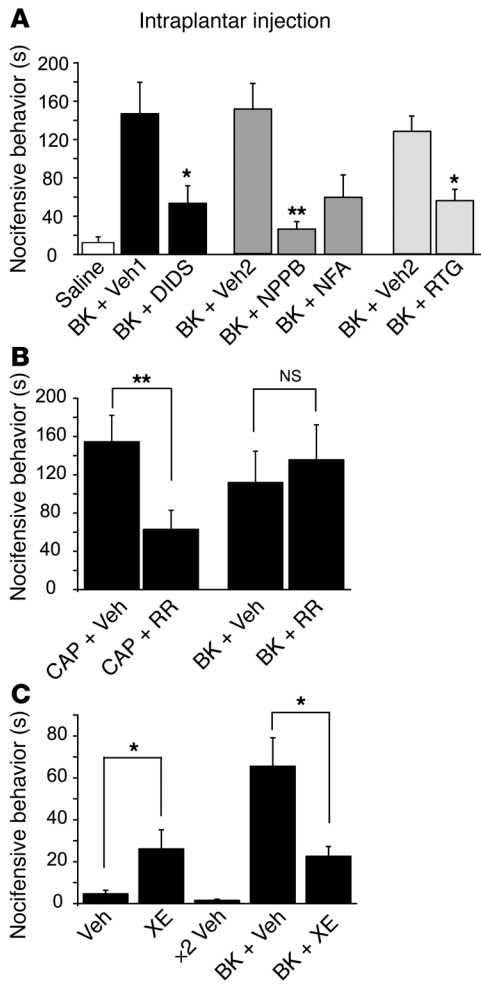
Figure 7
M channel inhibition and CaCC activation account for the BK-induced excitability in small DRG neurons. Current clamp recordings from small DRG neurons; APs were elicited by 200 pA current injection for a 500-ms period. (**A**) Under symmetrical Cl$^-$ conditions (high [Cl$^-$]$_i$ pipette solution), XE991 (3 μM) increased the number of APs elicited by the depolarizing current injection; subsequent application of 200 nM BK (together with XE991) further increased firing frequency; $n = 5$. (**B**) Experiment similar to **A**, but performed with low [Cl$^-$]$_i$ pipette solution. Under such conditions, application of BK does not cause any additional increase in XE991-induced AP firing; $n = 6$. (**C**) Another experiment with low [Cl$^-$]$_i$ pipette solution; this time, BK was applied first. In this case, BK was able to produce some excitation; subsequent application of XE991 (in the presence of BK) produced an additional increase in firing; $n = 4$. Bar charts at the bottom summarize the effects shown above; $*P \leq 0.05$, $**P \leq 0.01$.

RR had no effect on either the peak Ca^{2+} rise or area/peak parameter (Figure 6, F and G), while the more specific TRPV1 blocker capsazepine (10 μM) had a small but significant effect on the second-phase Ca^{2+} rise (but not on the peak rise; Figure 6, E–G). In contrast, the nonspecific voltage-gated Ca^{2+} channel (VGCC) blocker Ni^{2+}, as well as a cocktail of specific N-, P/Q-, T-, and L-type Ca^{2+} channel blockers and toxins (see Methods), significantly reduced both the peak and the second phase of the BK-induced Ca^{2+} rise (with a proportionally greater effect on the second phase; Figure 6, E–G). NFA (100 μM) also substantially reduced the second-phase and peak Ca^{2+} rises, suggesting that Cl$^-$ channel–mediated depolarization may contribute to these rises. These results suggest that VGCCs significantly contribute to the BK-induced Ca^{2+} rises, particularly to the second phase. We also tested whether AP firing is necessary for VGCC activation during the second phase of the Ca^{2+} response by treating neurons with a combination of tetrodotoxin (TTX, 1 μM) and A-803467 (100 nM) to block TTX-sensitive and -insensitive voltage-gated sodium channels (VGSCs) (34). This combination of VGSC inhibitors effectively blocked AP firing in small DRG neurons (data not shown); however, it did not significantly affect either the peak or the second phase of the Ca^{2+} signals (Figure 6G). Taken together, the results of Figure 1, D and E, and of Figure 6 suggest that the BK-induced Ca^{2+} signal is complex in nature and that the primary event is the release of Ca^{2+} from intracellular stores, which triggers a secondary Ca^{2+} influx, mainly through VGCCs that are activated by depolarization caused by the primary Ca^{2+} release. AP firing does not seem to be necessary for this VGCC activation. The contribution of TRP channels to acute BK-induced Ca^{2+} signals is small even at 37°C; however, the involvement of other RR-insensitive cationic channels cannot be excluded.

Since VGCCs in small DRG neurons are activated during the second phase of BK-induced Ca^{2+} signals, we tested whether Ca^{2+} influx through VGCCs can in turn activate CaCCs. Andre and

colleagues have reported that in medium and large mouse DRG neurons, CaCCs indeed can be activated by VGCC-mediated Ca^{2+} influx; however, in small neurons, VGCC-coupled CaCC current was not found (26). In our study (and also in ref. 35), CaCC current in CAP-positive nociceptors was activated by BK-induced Ca^{2+} transients; we thus asked whether this CaCC current can also be activated by VGCC-mediated Ca^{2+} influx. We performed fast whole-cell recordings using solutions and voltage protocols as in ref. 26. Consistent with the previous study, we found that in the majority (34 of 44) of small CAP-positive neurons, VGCC activation did not result in CaCC activation (Supplemental Figure 8A). In only 10 of 44 neurons, variable inward "tail" currents developed after the VGCC-activating pre-pulse (Supplemental Figure 8, B and C); these tail currents were sensitive to 100 μM NFA (data not shown). We concluded that in most small DRG neurons (in contrast to the medium/large ones), the coupling between VGCC and CaCC is minimal, which may suggest either poor spatial colocalization of CaCCs and VGCCs or a different molecular identity of CaCCs in small compared with large DRG neurons. Of note is also the fact that our voltage protocol for measuring M current involves repetitive stepping from –20 to –60 mV, a protocol that is likely to activate VGCCs; however, in perforated patch recordings M currents usually do not exhibit noticeable rundown, suggesting that Ca^{2+} influx through VGCCs in DRG neurons is not capable of producing noticeable inhibition of M channels either.

All experiments on M current inhibition and CaCC activation described above were performed on cultured neurons from P7 rats. Could we apply our findings to native neurons from adult animals? Robust M currents were reported in DRG neurons from P17 (20) and from 6-week-old adult rats (21); moreover, we recently reported that M current can be recorded from acute DRG slices, and this current can be inhibited by the activation of PLC (22). However, no such data exist for TMEM16A/CaCC (although strong TMEM16A immunoreactivity in small DRG neurons of adult mice has been

Figure 8

M channel openers and CaCC blockers attenuate BK-induced nocifensive behavior. (**A**) Cl⁻ channel blockers NPPB (10 nmol/site), NFA (50 nmol/site), DIDS (50 nmol/site), or M channel opener retigabine (RTG, 5 nmol/site) or vehicles (DMSO, Veh1; NaHCO₃, Veh2) were dissolved in saline and injected into the rat hind paw 5 minutes before the injection of BK (10 nmol/site) or saline in 50 μl (second injection was done into the same site). Nocifensive behavior was quantified as the time spent licking, biting, and flinching during 30 minutes. $n = 7$ for each group. (**B**) RR attenuated CAP- but not BK-induced nocifensive behavior. RR (50 nmol/site) or vehicle were preinjected 5 minutes prior to CAP or BK injection; $n = 8$ for each group. (**C**) Injection of M channel blocker XE991 (30 nmol/site) induced nocifensive behavior and attenuated BK-induced nociception. XE991 or vehicle control were injected into the plantar surface of the right hind paw either on their own or as pretreatment prior to BK injection; $n = 7$ for each group. *$P \leq 0.05$; **$P \leq 0.01$.

ure 9, A–C) or when BK and XE991 were coapplied after the first application of XE991 only (3.0 ± 0.4 AP/500 ms in the presence of XE991 only versus 8.8 ± 2.0 AP/500 ms in the presence of BK plus XE991, $n = 5$, $P \leq 0.05$; Figure 7A). These data suggest that both BK and XE991 can depolarize DRG neurons and increase AP firing frequency; however, under symmetrical Cl⁻ conditions, the effect of BK is stronger and contains a component that cannot be accounted for by the inhibition of M channels.

To test whether CaCC activation contributes to the excitatory effect of BK, we used a low [Cl⁻]ᵢ pipette solution, which abolished the BK-induced inward current. Under such conditions, the ability of XE991 (3 μM) to increase AP firing was unchanged (an increase from 1.4 ± 0.4 AP/500 ms to 5.0 ± 1.0 AP/500 ms, $n = 6$, $P \leq 0.05$; Figure 7B), while subsequent coapplication of BK plus XE991 failed to produce further excitation (4.6 ± 1.1 AP/500 ms, $n = 6$; Figure 7B). Moreover, at low [Cl⁻]ᵢ, BK (which inhibits some 50% of M current), when applied alone, was less potent in increasing AP firing than BK plus XE991 (with XE991 inhibiting M current almost completely; 2.8 ± 0.3 AP/500 ms in the presence of BK only versus 4.8 ± 0.8 AP/500 ms in the presence of BK plus XE991, $n = 4$, $P \leq 0.05$; Figure 7C). Taken together, these experiments demonstrate that both M current inhibition and CaCC activation contribute to the acute excitatory action of BK on sensory neurons; moreover, the combination of both effects can satisfactorily account for such action.

M channel openers and CaCC blockers can reduce nocifensive behavior induced by BK. We next tested whether pharmacological targeting of M channels and CaCC can influence BK-induced nocifensive behavior in rats. We evaluated nocifensive behavior (time spent licking, biting, and flinching the affected paw) after hind paw injection of 50 μl of saline containing the relevant compounds. Consistent with previous literature (2), intraplantar injection of BK (10 nmol/site) into the rat hind paw produced strong nocifensive behavior (quantified within the first 30 minutes after injection), which was not observed in rats injected with saline (Figure 8A). In order to investigate whether M channel inhibition or CaCC activation contributes to BK-induced nocifensive behavior, we preinjected the M channel opener retigabine or different CaCC blockers into the same plantar region of the hind paw where 5 minutes later BK was injected. This protocol limits central effects of the drugs and ensures that the preinjected drugs act on the same sensory neuron terminals as BK. We first tested whether the M channel opener retigabine can reduce BK-induced nocifensive behavior. We reasoned that M channels inhibited by BK might be "rescued" with retigabine. Retigabine (5 nmol/site) indeed

reported; ref. 32). Thus, we tested whether BK-induced inward current can be recorded in acutely dissociated DRG neurons from adult rats. Consistent with the data shown in Figure 3, BK induced robust Cl⁻-selective inward currents in small DRG neurons from 8-week-old adult rats just 4 hours after dissociation (Supplemental Figure 5B). In addition, the levels of *Tmem16a* transcript were similar in DRG cultures and acutely dissociated DRGs from adult rats (Figure 5F).

M current inhibition and CaCC activation contribute to and can account for the excitatory effect of BK. We examined how the effects of BK on M channels and CaCCs affect the excitability of small DRG neurons. In control neurons under current-clamp conditions (amphotericin B–perforated patch recording with regular, high [Cl⁻]ᵢ pipette solution), injection of 200 pA depolarizing current usually elicited only 1 or 2 APs (Figure 7A and Supplemental Figure 9, A and B). AP firing frequency was remarkably increased by 200 nM BK from 2.0 ± 0.6 AP/500 ms to 6.6 ± 1.3 AP/500 ms ($n = 7$, $P \leq 0.01$; Supplemental Figure 9A). BK also substantially depolarized the membrane potential from –56.8 ± 2.3 mV to –44.0 ± 3.0 mV ($n = 9$, $P \leq 0.01$; Supplemental Figure 9C). The specific M channel blocker XE991 (3 μM) also significantly increased the AP firing frequency from 1.4 ± 0.3 AP/500 ms to 4.1 ± 0.7 AP/500 ms ($n = 11$, $P \leq 0.01$; Supplemental Figure 9B) and induced depolarization from –55.7 ± 2.4 mV to –42.7 ± 2.5 mV ($n = 15$, $P \leq 0.01$; Supplemental Figure 9D). However, the number of APs elicited by the application of XE991 was smaller than that induced by BK (Supplemental Fig-

significantly attenuated BK-induced pain responses (Figure 8A). Accordingly, in patch-clamp experiments, application of retigabine effectively reversed the inhibitory effect of BK on M current at –60 mV (Supplemental Figure 5E).

We then tested whether pharmacological inhibition of CaCC would also have an anti-nocifensive effect. Preinjection of the Cl⁻ channel blockers DIDS (50 nmol/site) and NPPB (10 nmol/site) indeed significantly attenuated the BK-induced nocifensive behavior; NFA (50 nmol/site) also had a tendency to reduce the effect of BK (Figure 8A). We also tested the potential antinociceptive effect of RR. Intraplantar preinjection of RR (50 nmol/site) had no effect on BK-induced nociception (Figure 8B); however, as expected, RR did attenuate the nocifensive behavior produced by intraplantar injection of CAP (3 μg/site). Finally, we tested the nociceptive effect of peripheral M channel inhibition. In accordance with our previous study (22), intraplantar injections of XE991 (30 nmol/site) alone induced moderate nocifensive behavior (Figure 8C). Coinjection of XE991 with BK did not result in additional nocifensive responses; rather, there appeared to be a reduction in the pain response, which possibly may have resulted from desensitization of peripheral terminals caused by XE991-mediated sustained depolarization. These data suggest that M channel inhibition does not add any additional component to BK-induced nociception.

Discussion

M channels and BK-induced excitability in sensory neurons. M channels (Kv7 or KCNQ) conduct slow-kinetic, non-inactivating K⁺ currents with a threshold for activation below –60 mV, allowing a fraction of M channels to remain open at or near the resting membrane potential of a neuron. It is therefore suggested that neuronal M current serves as an intrinsic "voltage clamp" mechanism that controls the resting membrane potential, threshold for AP firing, and accommodation within AP trains (23). Accordingly, M channel inhibition depolarizes neurons, making them more excitable, while M current augmentation has the opposite effect (20, 36–38). Growing evidence suggests that functional M channels are expressed in peripheral sensory fibers and their activity strongly contributes to fiber excitability in vivo (22, 39–42). Here we show that BK inhibits M current in nociceptors, that M current inhibition is excitatory and causes nociception, and that the nociceptive effect of BK could be attenuated by the pre-application of a specific M channel opener (Figure 8).

$G_{q/11}$-coupled receptors can inhibit M currents via PLC-induced PIP₂ depletion (as M channels require PIP₂ for their activity; refs. 43–45), IP₃-mediated Ca²⁺ rises (as M channels are inhibited by Ca²⁺/calmodulin; refs. 46, 47), or a combination of both (48). Our data suggest that in DRG neurons, the Ca²⁺-mediated pathway prevails. Indeed, pharmacological inhibition of Ca²⁺ release from IP₃-sensitive stores or chelating intracellular Ca²⁺ with BAPTA (Figure 2) were almost as effective in preventing BK-induced M current inhibition as direct PLC inhibition. Imaging experiments (Figure 1) also suggest that despite activation of PLC by B₂R, the overall membrane PIP₂ level in most DRG neurons may not change dramatically, since YFP-tubby (PIP₂ reporter that does not bind IP₃; ref. 19) did not translocate in response to BK application (until B₂Rs were overexpressed).

New role of CaCCs in nociceptors. CaCCs are a prominent group of ion channels robustly expressed in many mammalian cell types, including neurons, smooth muscle and epithelial cells (49). In the nervous system, functional CaCCs are best characterized in neurons

mediating different sensory inputs, such as olfactory neurons (50, 51) or photosensitive rods and cones (52, 53), where these channels amplify excitatory inputs (e.g., the response to odorants mediated by Ca²⁺ influx through opening of CNG channels; ref. 54).

A critical prerequisite for Cl⁻ channels to conduct a depolarizing inward current is an equilibrium potential for Cl⁻ (E_{Cl}) that is more positive than the resting membrane potential of a neuron (–80 to –55 mV). In an archetypal CNS neuron, [Cl⁻]$_i$ is low and E_{Cl} is more negative than the resting membrane potential, so the activation of Cl⁻ channels (e.g., GABA) has a hyperpolarizing (inhibitory) effect. This, however, may not hold true for many types of sensory neurons, and there is evidence that there is a higher tonic [Cl⁻]$_i$ in peripheral sensory neurons, leading to E_{Cl} values in the range of –50 to –10 mV (refs. 55, 56 and the present study), which is well above the resting membrane potential. In our experiments on small nociceptive DRG neurons, both GABA and CaCC currents reversed at –35 mV to –40 mV (Figure 4). A recent report suggests that even further [Cl⁻]$_i$ accumulation in DRG neurons occurs in response to inflammation (55). In current clamp experiments (Figure 7 and Supplemental Figure 9), we clearly observed that under high [Cl⁻]$_i$ conditions, CaCC activation can amplify the excitatory effect of BK. Accordingly, intraplantar preinjection of CaCC blockers attenuated BK-induced nocifensive behavior in rats (Figure 8).

The molecular identity of CaCC remained controversial until very recently, when 3 groups independently identified a member of the transmembrane protein 16 (TMEM16 or anoctamin) protein family as a CaCC subunit (30–32). Most recently, another member of this family, TMEM16B was also shown to have CaCC activity (57). We still know little about the structural basis for the Cl⁻ conductance and Ca²⁺ sensitivity of TMEM16A, but its identification as a molecular correlate of CaCC makes it possible to alter CaCCs in native cells via genetic manipulation. In this study, we detected TMEM16A immunoreactivity in TRPV1-positive DRG neurons (Supplemental Figures 1 and 7) and used the siRNA approach to show that *Tmem16a* knockdown reduces CaCC currents in these cells (Figure 5). We also detected *Tmem16b* expression in total DRG culture extracts, but its level of expression was approximately 100 times lower than that of *Tmem16a*.

An apparently different type of endogenous CaCC current has been reported in medium/large DRG neurons. This CaCC current was reported to couple to VGCC activation (26), while in the case of CaCC in small DRG neurons, such coupling is weak (the present study). Such a lack of coupling between CaCC and VGCC in nociceptors may be required in order to avoid a self-maintaining positive feedback loop, since if Ca²⁺ influx through VGCC would significantly activate CaCC (and inhibit M channels), this would then cause depolarization and Ca²⁺ influx through VGCC and further amplification of the cycle. Interestingly, *Tmem16a* is highly expressed in the majority of small DRG neurons but not in large neurons (32); moreover, it was recently suggested that *Best1* underlies CaCC in large neurons (58). Taken together, these two observations may indicate that CaCC in different types of neurons consist of distinct molecular components.

Contribution of other currents to the acute effect of BK. In our experiments, the inhibition of M current and activation of CaCC were the most prominent effects of BK on ionic currents in DRG neurons; moreover, these effects satisfactorily accounted for the observed excitatory action of BK. Our data suggest that the contribution of TRP channels to the acute effects of BK in nociceptors

is not large, as the non-Cl⁻ component of the BK-induced inward currents was small even at 37°C (Figure 6); overexpression of B_2Rs in DRG neurons also did not result in large non-Cl⁻ BK-activated currents; finally, TRP channel blockers had little effect on BK-induced Ca^{2+} transients (Figure 6) or nociceptive behavior (Figure 8). Our results seem at odds with publications suggesting that BK can activate TRPV1 (59, 60) and TRPA1 (61). Nevertheless we confirmed the sensitizing effect of BK on TRPV1 via endogenous B_2Rs; moreover, small non-Cl⁻ inward currents in response to BK recorded at 37°C suggest that some degree of sensory TRP channel activation by BK may happen in vivo. We believe that in our experimental conditions, B_2R indeed produced some sensitization of sensory TRP channels, but the overall contribution of this effect to the acute BK-induced excitability and nociception was small. A recent report suggested that acute BK-induced nocifensive behavior in *Trpv1*-knockout mice was affected only marginally (62). The study tested two doses of BK, 0.1 and 1 nmol/site; the behavioral responses to BK did not differ between wild-type and *Trpv1⁻/⁻* animals at a higher BK dose, and at a lower dose the percentage of BK-responsive animals was smaller in the *Trpv1⁻/⁻* group, but the amount of distress experienced by the responsive animals did not change significantly. Moreover, BK-induced excitation of cutaneous C fibers was similar in wild-type and *Trpv1⁻/⁻* mice at a range of BK concentrations. Thus, we suggest that B_2R-TRP coupling may have a stronger role in the BK-induced hyperalgesia/allodynia than in the acute nociception produced by BK.

General principles of spontaneous inflammatory nociception. Inflammatory mediators (such as BK, proteases, histamine, prostaglandins, IL1-β, ATP, NGF, etc.) often act via G protein–coupled receptors or ligand-gated ion channels to acutely depolarize the plasma membrane of sensory fibers, reduce the threshold for AP firing, and increase firing frequency (3). Our data as well as emerging work from many other research groups allow us to propose certain common principles underlying the "spontaneous" excitation of peripheral sensory neurons in inflammation: (a) weakening of intrinsic "voltage clamp" — e.g., through M channel inhibition (ref. 22 and the present study); (b) depolarizing input — e.g., through activation of cationic channels such as P_2X (63) and TRP (61, 64) or anionic channels such as CaCCs (the present study); (c) amplification of the depolarizing input — e.g., by the upregulation of VGSCs (65, 66) or by positive feedback activation of CaCCs.

Methods

The use of animals in this study was approved by the University of Leeds Ethical Review Committee and by the Animal Care and Ethical Committee of Hebei Medical University.

Rat DRG cell culture. DRGs were extracted from all spinal levels of 7-day-old Wistar rats, and neurons were dissociated and cultured as described previously (22, 67). For preparation of purified DRG culture, see Supplemental Methods.

Electrophysiology. Unless stated otherwise, recordings were made at room temperature. Patch electrodes were pulled from borosilicate glass and fire-polished to a final resistance of 2–4 MΩ when filled with internal solution. An EPC-10 patch clamp amplifier in combination with Patchmaster version 2.2 software (HEKA) was used for voltage and current clamp experiments. Most recordings were done using either amphotericin B– (250 µg/ml; Sigma-Aldrich) or gramicidin-perforated (100 µg/ml; Sigma-Aldrich) patch technique. Regular (high $[Cl^-]_i$) internal pipette solution contained (in mM): 150 KCl, 5 $MgCl_2$, 10 HEPES, pH 7.4. In the low $[Cl^-]_i$ pipette

solution, KCl was replaced by equimolar K-acetate. Calcium clamping experiments were done using fast whole-cell recording using the following "high BAPTA" internal solution (in mM): 115 KCl, 5 $MgCl_2$, 5 HEPES, 20 BAPTA, 3 K_2ATP, 0.1 NaGTP, and 10 $CaCl_2$, pH 7.4. The external solution contained (in mM) 160 NaCl, 2.5 KCl, 5 $CaCl_2$, 1 $MgCl_2$, 10 HEPES, and 8 glucose, pH 7.4. A low-profile perfusion chamber fed by a gravity perfusion system was used for solution exchange (2 ml/min, bath exchange time of ~15 seconds). M current amplitude was measured from the deactivation current elicited by a 500-ms square voltage pulse to –60 mV from a holding potential of –20 mV or –30 mV, calculated as the difference between the average of a 10-ms segment, taken 20–30 ms into the hyperpolarizing step, and the average during the last 50 ms of that step. Additional details are provided in Supplemental Methods.

Fluorescence imaging. Ca^{2+} imaging was performed as described previously (46); briefly, neurons were loaded with fura-2AM (2 µM) in the presence of Pluronic F-127 (0.02%) and imaged using a Nikon TE-2000 microscope (10× objective) equipped with a T.I.L.L. Photonics Ca^{2+} imaging system (Polychrome V monochromator and IMAGO CCD camera). Cells were excited alternatively at 340 and 380 nm and images analyzed with TILLvisION 4.5.56. Only neurons responding with a greater than 10% rise (peak) in F340/F380 were counted as BK positive. The area/peak parameter in Figure 6F was calculated according to the following equation:

$$(\int_a^b R/R_0 - 1)/(R_{peak}/R_0)$$

(Equation 1)

where *a* and *b* are the start and end points of the Ca^{2+} transient (Figure 6F, inset).

Translocation of PIP_2 probes was recorded using a LiveScan Swept Field Confocal System (Nikon) as in ref. 22, and data were analyzed using NIS Elements imaging software (Nikon).

DNA constructs, siRNA, and transfections. Freshly isolated DRG neurons were transfected with PLC_δ-PH-GFP (gift from Tobias Meyer, Stanford University, California) or YFP-tubby (tubby-R332H-cYFP; gift from Andrew Tinker, UCL, London, United Kingdom) with or without B_2R (gift from Mark Shapiro, UT Health Science Center San Antonio, Texas) using a Nucleofector device (Amaxa) and used 3–5 days after transfection. siRNA oligonucleotide sequences against *Tmem16a* (with matching scrambled controls) were designed using BLOCK-iT RNAi designer (Invitrogen): siRNA sense, CCUGGUCAGGAAAUACUUU[dT][dT], antisense, AAAG UAUUUCCUGACCAGG[dT][dT]; scrambled 1 sense, CCUACUAGGUAA CAGGUUU[dT][dT], antisense, AAACCUGUUACCUAGUAGG[dT][dT]; scrambled 2 sense, GCAGUAUUCCGAUAGACUU[dT][dT], antisense, AAGUCUAUCGGAAUACUGC[dT][dT]. Amaxa's Nucleofector device was used for siRNA delivery; the efficiency of *Tmem16a* knockdown was checked by quantitative RT-PCR (Bio-Rad), immunocytochemistry, and Western blot analysis (see Supplemental Methods). In patch-clamp experiments, RNA oligos were cotransfected with EGFP cDNA, and neurons with green fluorescence were analyzed.

Behavioral studies. Sprague-Dawley rats (body weight, 190–240 g) were randomly grouped and allowed to acclimatize for at least 20 minutes in a transparent observation chamber before the experiment. The right hind paw of the animal received an intraplantar injection (50 µl) of BK (10 nmol/site) or vehicle, and the nocifensive responses (licking, biting, lifting, and flinching) were recorded using a video camera for 30 minutes. The videos were analyzed by an observer unaware of treatment allocations. In the experiments with M channel openers and CaCC or TRP blockers, these drugs were preinjected in the same plantar of the hind paw where 5 minutes later BK was injected. Drugs were dissolved in saline (pH 7.4) from stock solu-

tions and applied in a volume of 50 μl at the following doses: retigabine, 5 nmol/site; DIDS, 50 nmol/site; NPPB, 10 nmol/site; NFA, 50 nmol/site; CAP, 3 μg/site; RR, 50 nmol/site; XE991, 30 nmol/site.

Statistics. The concentration-response curve was fitted with logistic equation: $y = A_2 + (A_1 - A_2)/[1 + (x/x_0)^p]$, where y is the response; A_1 and A_2 are the maximum and minimum response, respectively, x is the drug concentration, and p is the Hill coefficient. All data are given as mean ± SEM. Differences between groups were assessed by Student's t test or 1-way ANOVA. The differences were considered significant at $P \leq 0.05$.

Chemicals. Edelfosine was from Calbiochem; XE991 and ZD7288, from Tocris; Xe-C, from Cayman Europe; and fura-2AM, from Invitrogen. Retigabine was a gift from Kewei Wang (Peking University, Beijing, China); all other chemicals were from Sigma-Aldrich.

Address correspondence to: Nikita Gamper, Institute of Membrane and Systems Biology, Faculty of Biological Sciences, University of Leeds, LS2 9JT Leeds, United Kingdom. Phone: 44.113.343.7923; Fax: 44.113.343.3167; E-mail: n.gamper@leeds.ac.uk. Or to: Hailin Zhang, Department of Pharmacology, Hebei Medical University, 361 Zhongshan East Road, Shijiazhuang 050017, China. Phone: 86.311.86265562; Fax: 86.311.86057291; E-mail: zhanghl@hebmu.edu.cn.

Boyi Liu's present address is: Department of Pharmacology, Yale University School of Medicine, New Haven, Connecticut.

1. Keele CA. The chemistry of pain production. *Proc R Soc Med.* 1967;60(4):419–422.
2. Dray A, Perkins M. Bradykinin and inflammatory pain. *Trends Neurosci.* 1993;16(3):99–104.
3. McMahon SB, Bennet DLH, Bevan S. Inflammatory mediators and modulators. In: McMahon SB, Koltzenburg M, eds. *Wall and Melzack's Textbook of Pain.* Edinburgh, United Kingdom: Elsevier Churchill Livingstone. 2006:49–72.
4. Raidoo DM, Bhoola KD. Pathophysiology of the kallikrein-kinin system in mammalian nervous tissue. *Pharmacol Ther.* 1998;79(2):105–127.
5. Couture R, Harrisson M, Vianna RM, Cloutier F. Kinin receptors in pain and inflammation. *Eur J Pharmacol.* 2001;429(1–3):161–176.
6. Chuang HH, et al. Bradykinin and nerve growth factor release the capsaicin receptor from PtdIns(4,5)P2-mediated inhibition. *Nature.* 2001;411(6840):957–962.
7. Wang S, et al. Phospholipase C and protein kinase A mediate bradykinin sensitization of TRPA1: a molecular mechanism of inflammatory pain. *Brain.* 2008;131(Pt 5):1241–1251.
8. Cesare P, Dekker LV, Sardini A, Parker PJ, McNaughton PA. Specific involvement of PKC-epsilon in sensitization of the neuronal response to painful heat. *Neuron.* 1999;23(3):617–624.
9. Mandadi S, et al. Increased sensitivity of desensitized TRPV1 by PMA occurs through PKCepsilon-mediated phosphorylation at S800. *Pain.* 2006;123(1–2):106–116.
10. Burgess GM, Mullaney I, McNeill M, Dunn PM, Rang HP. Second messengers involved in the mechanism of action of bradykinin in sensory neurons in culture. *J Neurosci.* 1989;9(9):3314–3325.
11. Dray A, Patel IA, Perkins MN, Rueff A. Bradykinin-induced activation of nociceptors: receptor and mechanistic studies on the neonatal rat spinal cord-tail preparation in vitro. *Br J Pharmacol.* 1992;107(4):1129–1134.
12. Oh EJ, Weinreich D. Bradykinin decreases K⁺ and increases Cl⁻ conductances in vagal afferent neurones of the guinea pig. *J Physiol.* 2004;558(Pt 2):513–526.
13. Gamper N, Shapiro MS. Target-specific PIP2 signaling: how might it work? *J Physiol.* 2007;582(Pt 3):967–975.
14. Gamper N, Shapiro MS. Regulation of ion transport proteins by membrane phosphoinositides. *Nat Rev Neurosci.* 2007;8(12):921–934.
15. Stauffer TP, Ahn S, Meyer T. Receptor-induced transient reduction in plasma membrane PtdIns(4,5)P2 concentration in living cells. *Curr Biol.* 1998;8(6):343–346.
16. Hirose K, Kadowaki S, Tanabe M, Takeshima H, Iino M. Spatiotemporal dynamics of inositol 1,4,5-trisphosphate that underlies complex Ca²⁺ mobilization patterns. *Science.* 1999;284(5419):1527–1530.
17. Varnai P, Balla T. Visualization of phosphoinositides that bind pleckstrin homology domains: calcium- and agonist-induced dynamic changes and relationship to myo-[3H]inositol-labeled phosphoinositide pools. *J Cell Biol.* 1998;143(2):501–510.
18. Gamper N, Reznikov V, Yamada Y, Yang J, Shapiro MS. Phosphatidylinositol 4,5-bisphosphate signals underlie receptor-specific Gq/11-mediated modulation of N-type Ca²⁺ channels. *J Neurosci.* 2004;24(48):10980–10992.
19. Quinn KV, Behe P, Tinker A. Monitoring changes in membrane phosphatidylinositol 4,5-bisphosphate in living cells using a domain from the transcription factor tubby. *J Physiol.* 2008;586(Pt 12):2855–2871.
20. Passmore GM, et al. KCNQ/M currents in sensory neurons: significance for pain therapy. *J Neurosci.* 2003;23(18):7227–7236.
21. Crozier RA, Ajit SK, Kaftan EJ, Pausch MH. MrgD activation inhibits KCNQ/M-currents and contributes to enhanced neuronal excitability. *J Neurosci.* 2007;27(16):4492–4496.
22. Linley JE, Rose K, Patil M, Robertson B, Akopian AN, Gamper N. Inhibition of M current in sensory neurons by exogenous proteases: a signaling pathway mediating inflammatory nociception. *J Neurosci.* 2008;28(44):11240–11249.
23. Delmas P, Brown DA. Pathways modulating neural KCNQ/M (Kv7) potassium channels. *Nat Rev Neurosci.* 2005;6(11):850–862.
24. Heblich F, England S, Docherty RJ. Indirect actions of bradykinin on neonatal rat dorsal root ganglion neurones: a role for non-neuronal cells as nociceptors. *J Physiol.* 2001;536(Pt 1):111–121.
25. Mayer ML. A calcium-activated chloride current generates the after-depolarization of rat sensory neurones in culture. *J Physiol.* 1985;364:217–239.
26. Andre S, et al. Axotomy-induced expression of calcium-activated chloride current in subpopulations of mouse dorsal root ganglion neurons. *J Neurophysiol.* 2003;90(6):3764–3773.
27. Ward SM, Kenyon JL. The spatial relationship between Ca²⁺ channels and Ca²⁺-activated channels and the function of Ca²⁺-buffering in avian sensory neurons. *Cell Calcium.* 2000;28(4):233–246.
28. Ebihara S, Shirato K, Harata N, Akaike N. Gramicidin-perforated patch recording: GABA response in mammalian neurones with intact intracellular chloride. *J Physiol.* 1995;484(Pt 1):77–86.
29. Chabwine JN, et al. Differential contribution of the Na⁺-K⁺-2Cl⁻ cotransporter NKCC1 to chloride handling in rat embryonic dorsal root ganglion neurons and motor neurons. *FASEB J.* 2009;23(4):1168–1176.
30. Caputo A, et al. TMEM16A, a membrane protein associated with calcium-dependent chloride channel activity. *Science.* 2008;322(5901):590–594.
31. Schroeder BC, Cheng T, Jan YN, Jan LY. Expression cloning of TMEM16A as a calcium-activated chloride channel subunit. *Cell.* 2008;134(6):1019–1029.
32. Yang YD, et al. TMEM16A confers receptor-activated calcium-dependent chloride conductance. *Nature.* 2008;455(7217):1210–1215.
33. Sugiura T, Tominaga M, Katsuya H, Mizumura K. Bradykinin lowers the threshold temperature for heat activation of vanilloid receptor 1. *J Neurophysiol.* 2002;88(1):544–548.
34. Jarvis MF, et al. A-803467, a potent and selective Nav1.8 sodium channel blocker, attenuates neuropathic and inflammatory pain in the rat. *Proc Natl Acad Sci U S A.* 2007;104(20):8520–8525.
35. Lee MG, Macglashan DW Jr, Undem BJ. Role of chloride channels in bradykinin-induced guinea pig airway vagal C-fibre activation. *J Physiol.* 2005;566(Pt 1):205–212.
36. Gamper N, et al. Oxidative modification of M-type K⁺ channels as a mechanism of cytoprotective neuronal silencing. *EMBO J.* 2006;25(20):4996–5004.
37. Jones S, Brown DA, Milligan G, Willer E, Buckley NJ, Caulfield MP. Bradykinin excites rat sympathetic neurons by inhibition of M current through a mechanism involving B2 receptors and G alpha q/11. *Neuron.* 1995;14(2):399–405.
38. Shah MM, Migliore M, Valencia I, Cooper EC, Brown DA. Functional significance of axonal Kv7 channels in hippocampal pyramidal neurons. *Proc Natl Acad Sci U S A.* 2008;105(22):7869–7874.

39. Blackburn-Munro G, Jensen BS. The anticonvulsant retigabine attenuates nociceptive behaviours in rat models of persistent and neuropathic pain. *Eur J Pharmacol*. 2003;460(2-3):109–116.

40. Hirano K, Kuratani K, Fujiyoshi M, Tashiro N, Hayashi E, Kinoshita M. Kv7.2-7.5 voltage-gated potassium channel (KCNQ2-5) opener, retigabine, reduces capsaicin-induced visceral pain in mice. *Neurosci Lett*. 2007;413(2):159–162.

41. Lang PM, Fleckenstein J, Passmore GM, Brown DA, Grafe P. Retigabine reduces the excitability of unmyelinated peripheral human axons. *Neuropharmacology*. 2008;54(8):1271–1278.

42. Roza C, Lopez-Garcia JA. Retigabine, the specific KCNQ channel opener, blocks ectopic discharges in axotomized sensory fibres. *Pain*. 2008;138(3):537–545.

43. Li Y, Gamper N, Hilgemann DW, Shapiro MS. Regulation of Kv7 (KCNQ) K+ channel open probability by phosphatidylinositol (4,5)-bisphosphate. *J Neurosci*. 2005;25(43):9825–9835.

44. Suh B, Hille B. Recovery from muscarinic modulation of M current channels requires phosphatidylinositol 4,5-bisphosphate synthesis. *Neuron*. 2002;35(3):507–520.

45. Zhang H, et al. PIP2 activates KCNQ channels, and its hydrolysis underlies receptor-mediated inhibition of M currents. *Neuron*. 2003;37(6):963–975.

46. Gamper N, Shapiro MS. Calmodulin mediates Ca2+-dependent modulation of M-type K+ channels. *J Gen Physiol*. 2003;122(1):17–31.

47. Selyanko AA, Brown DA. Intracellular calcium directly inhibits potassium M channels in excised membrane patches from rat sympathetic neurons. *Neuron*. 1996;16(1):151–162.

48. Brown DA, Hughes SA, Marsh SJ, Tinker A. Regulation of M(Kv7.2/7.3) channels in neurons by PIP2 and products of PIP2 hydrolysis: significance for receptor-mediated inhibition. *J Physiol*. 2007;582(Pt 3):917–925.

49. Frings S, Reuter D, Kleene SJ. Neuronal Ca2+ -activated Cl- channels — homing in on an elusive channel species. *Prog Neurobiol*. 2000;60(3):247–289.

50. Kleene SJ, Gesteland RC. Calcium-activated chloride conductance in frog olfactory cilia. *J Neurosci*. 1991;11(11):3624–3629.

51. Lowe G, Gold GH. Nonlinear amplification by calcium-dependent chloride channels in olfactory receptor cells. *Nature*. 1993;366(6452):283–286.

52. Bader CR, Bertrand D, Schwartz EA. Voltage-activated and calcium-activated currents studied in solitary rod inner segments from the salamander retina. *J Physiol*. 1982;331:253–284.

53. Barnes S, Hille B. Ionic channels of the inner segment of tiger salamander cone photoreceptors. *J Gen Physiol*. 1989;94(4):719–743.

54. Menini A. Calcium signalling and regulation in olfactory neurons. *Curr Opin Neurobiol*. 1999;9(4):419–426.

55. Funk K, Woitecki A, Franjic-Wurtz C, Gensch T, Mohrlen F, Frings S. Modulation of chloride homeostasis by inflammatory mediators in dorsal root ganglion neurons. *Mol Pain*. 2008;4:32.

56. Gilbert D, Franjic-Wurtz C, Funk K, Gensch T, Frings S, Mohrlen F. Differential maturation of chloride homeostasis in primary afferent neurons of the somatosensory system. *Int J Dev Neurosci*. 2007;25(7):479–489.

57. Stohr H, et al. TMEM16B, a novel protein with calcium-dependent chloride channel activity, associates with a presynaptic protein complex in photoreceptor terminals. *J Neurosci*. 2009;29(21):6809–6818.

58. Boudes M, et al. Best1 is a gene regulated by nerve injury and required for Ca2+-activated Cl- current expression in axotomized sensory neurons. *J Neurosci*. 2009;29(32):10063–10071.

59. Premkumar LS, Ahern GP. Induction of vanilloid receptor channel activity by protein kinase C. *Nature*. 2000;408(6815):985–990.

60. Shin J, et al. Bradykinin-12-lipoxygenase-VR1 signaling pathway for inflammatory hyperalgesia. *Proc Natl Acad Sci U S A*. 2002;99(15):10150–10155.

61. Bandell M, et al. Noxious cold ion channel TRPA1 is activated by pungent compounds and bradykinin. *Neuron*. 2004;41(6):849–857.

62. Katanosaka K, et al. Contribution of TRPV1 to the bradykinin-evoked nociceptive behavior and excitation of cutaneous sensory neurons. *Neurosci Res*. 2008;62(3):168–175.

63. Xu GY, Huang LY. Peripheral inflammation sensitizes P2X receptor-mediated responses in rat dorsal root ganglion neurons. *J Neurosci*. 2002;22(1):93–102.

64. Dai Y, et al. Proteinase-activated receptor 2-mediated potentiation of transient receptor potential vanilloid subfamily 1 activity reveals a mechanism for proteinase-induced inflammatory pain. *J Neurosci*. 2004;24(18):4293–4299.

65. Maingret F, et al. Inflammatory mediators increase Nav1.9 current and excitability in nociceptors through a coincident detection mechanism. *J Gen Physiol*. 2008;131(3):211–225.

66. Binshtok AM, et al. Nociceptors are interleukin-1beta sensors. *J Neurosci*. 2008;28(52):14062–14073.

67. Liu B, Liang H, Liu L, Zhang H. Phosphatidylinositol 4,5-bisphosphate hydrolysis mediates histamine-induced KCNQ/M current inhibition. *Am J Physiol Cell Physiol*. 2008;295(1):C81–C91.